ORIGINAL PAPER

Hysteresis online identification approach for smart material actuators with different input signals and external disturbances

Sicheng Yi · Quan Zhang · Liang Xu · Tianhong Wang · Long Li

Abstract In this article, we present a fraction-order polynomial-modified Prandtl–Ishlinskii (FPMPI) and online infinite impulse response (OIIR) integrated model to describe the rate/load/temperature hystereses for smart material actuators. Hysteresis loops exhibit dynamic, asymmetric and saturate phenomena under different input rates, external loads and surrounding temperatures. It is difficult to apply a comprehensive model to accurately capture the hysteresis variation. The Hammerstein-based hysteresis offline identification study is conducted. It is found that the rate/load/temperature-dependent hysteresis cannot be described well via the offline approach, due to the system uncertainty and time-varying dynamics. By formulating the hysteresis modeling as an adaptive filtering problem, the OIIR filter and FPMPI integrated model is utilized for the rate/load/temperature-dependent hysteresis identification. Comparison of the online and offline identification results shows that the hysteresis online identification accuracies improve at least one order of magnitude, and two orders for some cases.

S. Yi · Q. Zhang (✉) · L. Xu · T. Wang · L. Li
School of Mechatronic Engineering and Automation,
Shanghai University, Shanghai, China
e-mail: lincolnquan@shu.edu.cn

S. Yi · Q. Zhang
Artificial Intelligence Institute, Shanghai University,
Shanghai, China

S. Yi
School of Mechanical Engineering, Shanghai Jiao Tong
University, Shanghai, China

1 Introduction

Smart materials actuators are progressively being investigated for micropositioning [1] and microvibration [2] control applications where fast reaction, large powers density, high resolution are required. The magnetostrictive, piezoelectric and shape memory alloy (SMA) actuators are considered potential. However, for those actuators, the output vs. input loops exhibit complicated hysteresis phenomena, which tend to be asymmetric, saturate and dynamic. The profile of the hysteresis loop is dependent on the amplitude/frequency/bias of the input signal, external load and surrounding temperature and so on [3,4]. To predict the response and develop the inversion-based feedforward control method for the smart material actuators [5–7], it is essential to exactly formulate the hysteresis model.

As to the rate-independent hysteresis model, the typical phenomenological modeling approaches include the Krasnosel'skii–Pokrovskii (KP) [8], Preisach [9] and Prandtl–Ishlinskii (PI) [10]. PI model has been more applied recently since it possesses a more simplified form compared against the KP and Preisach models. To account for the asymmetric effect of the rate-independent hysteresis, the integer-order polynomial [11,12], a Lipchitz continuous function, is applied

to modify the conventional PI model. In this paper, by analyzing the graph of the fractional-order polynomials, it can be found that it can be more effective than the integer-order polynomial in terms of asymmetric hysteresis modeling. We will apply the fractional-order polynomial-modified PI (FPMPI) model to characterize the rate-independent hysteresis.

It is difficult to build the rate-dependent hysteresis model over a wide range of frequencies. To the best of our knowledge, three kinds of approaches are proposed in previous studies. (i) The conventional hysteresis operators are modified [13–17]. In most cases, the weight or threshold function is changed to be rate-dependent. The down side is that the rate-dependent threshold function needs to hold the dilation condition. (ii) Some intelligent models based on fuzzy or machine learning theory are proposed to describe the rate-dependent hysteresis [18–20]. For those models, the complicated intelligent algorithms are required to realize the rate-dependent hysteresis modeling. (iii) A few hysteresis models based on the Hammerstein principle are presented [1,2,12,21,22]. For the Hammerstein-based modeling approach, the rate-independent hysteresis model is cascaded with the linear time-invariant (LTI) dynamics model. For those models, both the rate-independent and rate-dependent parts of the hysteresis are identified offline. The system uncertainty not considered for the hysteresis offline modeling approach may result in unmodeled error.

Compared with a lot of attention which is paid to the rate-dependent hysteresis modeling, the numbers of studies on load- and temperature-dependent hysteresis modeling approaches are relatively smaller. The reason is that experiments are usually conducted in the laboratories, where the load is often fixed or not applied and the surrounding temperature is often controlled. But in engineering, these environmental factors should be taken into key account. For example, the smart material actuators undergo load variation for robot manipulating application; they would operate in space environment of which the ambient temperature changes.

The external load plays effect upon the hysteresis loop of the smart material actuator [23,24]. Different methods have been applied to describe the load-dependent hysteresis. The coupled magneto-thermo-mechanical hysteresis models based on the constitutive principle are built [25,26] but not suitable for real-time control. A novel model based on neural networks is proposed [27] to describe the relation between the magne-tostrictive strain and magnetization strength for different loads. Nevertheless, the model accuracy improvement needs the large size of databases. The asymmetric shifted PI and load-dependent electromechanical models are combined to develop a comprehensive approach to describe the rate/load-dependent hysteresis for magnetostrictive positioner [28]. The approach relies on the specific physical system and is not general for other smart material actuators.

The temperature also plays effect upon the hysteresis of the smart material actuators. The hysteresis characterizations of the piezo-stack actuator for different temperatures are studied experimentally [3,29,30]. To describe the magnetic-elastic-thermal coupling behavior, a nonlinear transient constitutive model for magnetostrictive actuator is established [31]. However, the exact values of some parameters in this constitutive model cannot be acquired directly. A few studies have been performed to model the temperature-dependent hysteresis. A temperature-dependent Prandtl–Ishlinskii model (TD-PI) is proposed to account for the temperature effects on the hysteresis nonlinearity [3]. The difficulty is determination of temperature shape function. A model incorporating the thermal and piezoelectric sub-models is presented [30]. The thermal sub-model is established by the FEM method, resulting in a lot of computation for model identification.

It is a big challenge to establish and identify a hysteresis model totally incorporating those factors. To the best of our knowledge, most models are limited to describe one- or two-factor-dependent hysteresis in previous studies, for example, rate/temperature-dependent in [3], rate/load-dependent in [28]. The rate/load/temperature-dependent hystereses are described via a few multi-physics-field coupling modeling approaches [25,31]. But the physical hysteresis modeling process for a specific smart material actuator cannot be extended for other types of actuators. In this paper, we propose a data-driven identification technique; that is, the hysteresis is identified only based on the input/output data regardless of the specific type of the smart material actuator.

To the best of our knowledge, most of previous hysteresis modeling and identification approaches are based on offline technique. It is well known that the input and output data used for offline identification are processed in batch form by least squares, maximum likelihood or other parameter estimation methods.

Thus, a large amount of data needs to be stored and processed [32], particularly for the complex process like rate/load/temperature-dependent hysteresis identification. More importantly, the offline model is not much robust to the varying input signals and external disturbance. To this end, an online identification approach capable of tracking the actual rate/load/temperature-dependent hysteretic response is presented in this paper. In terms of the online identification technique, when the input and output data are updated in a sampling period, they are processed online by the recursive method. The online identification approach is more competitive than the offline one. First, the data stored and processed are smaller than the offline identification approach; secondly, it can address the problem of characterizing system uncertainty and time-varying dynamics which exist in the hysteretic system with different input signals and external disturbances.

The main contribution of this work is that a hysteresis online identification approach is proposed to describe the rate/load/temperature-dependent hysteresis. The remainder of this article starts by clarifying the problem of the system uncertainty and time-varying dynamics when the Hammerstein-based hysteresis offline modeling approach is applied to identify the rate/load/temperature-dependent hysteresis. The system uncertainty and time variation relying on input rates, external loads and/or surrounding temperatures are analyzed experimentally on the magnetostrictive and piezoelectric actuators. Then, we demonstrate the hysteresis online identification approach, where the dynamics of smart material actuators are modeled in real time considering the different input signals and external disturbances in Sect. 2. Section 3 presents the rate/load/temperature-dependent hysteresis online identification results, and they are compared against the offline ones. The hysteresis identification is performed on magnetostrictive, piezoelectric and SMA actuators. Finally, the content of this article is summarized and future studies are introduced.

2 Problem statement

2.1 Hammerstein-based hysteresis offline identification

Based on the Hammerstein principle, the hysteresis nonlinear model of smart material can be repre-
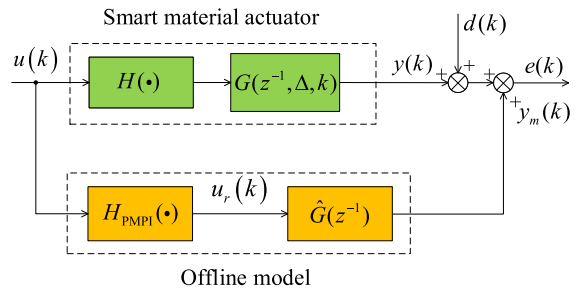
Fig. 1 Block diagram of the hysteresis offline identification approach for smart material actuator

sented by the cascade of the rate-independent and rate-dependent parts. As shown in Fig. 1, $u(k)$ and $y(k)$ are the input and actual output signals, respectively; $d(k)$ is the external disturbance induced by the environmental temperature or/and carrying load, etc.; $y_m(k)$ is the model output; $e(k)$ is the error signal which is the difference of the actual and modeled output signals; and $u_r(k)$ is the intermediate signal of the offline model. $H(\cdot)$ and $G(\cdot)$ are the rate-independent and rate-dependent subsystems, respectively. Δ and k denote the uncertainty and varying dynamics, respectively.

It is noted that the plant to be identified is a single-input single-output (SISO) one. The effect of external disturbance on the plant is reflected in the time-varying characteristics of the system. The subsystems can be identified offline using the polynomial-modified Prandtl–Ishlinskii and linear time-invariant dynamics sub-models, that is, $H_{\mathrm{PMPI}}(\cdot)$ and $\hat{G}(z^{-1})$, respectively. If there exist some uncertainty Δ in smart material actuator, for example, the unmodeled dynamics and unknown parameter, the hysteresis offline identification accuracy will be reduced. Meanwhile, if the external disturbances $d(k)$, e.g., carrying load $d_L(k)$ and surrounding temperature $d_T(k)$, affect the output of the smart material actuator, the offline-identified model cannot capture the disturbance-induced hysteresis variation accurately. In essence, the uncertainty Δ and time-variant dynamics $G(z^{-1}, k)$ are difficult to be described by the conventional hysteresis offline modeling approach.

It is noted that, in this paper, the input signals for magnetostrictive, piezoelectric and SMA actuators are current $i(k)$, voltage $v(k)$ and temperature $T(k)$. Their output signals are magnetostrictive displacement $\chi_m(k)$, piezoelectric displacement $\chi_p(k)$ and SMA rotation angle $\chi_s(k)$.

## 2.2 System uncertainty for the rate-dependent hysteresis

The rate-dependent properties of the hysteresis loops for the magnetostrictive and piezoelectric actuators are illustrated in Figs. 2 and 3, respectively. The former device is custom-developed, while the latter is produced by Harbin Core Tomorrow Science and Technology Co., Ltd. The specifications of both actuators are summarized in Table 1. As shown in Fig. 2a, the laser displacement sensor (LK-G80, Keyence Corporation) is installed to measure the magnetostrictive actuator displacement. The driven current of the magnetostrictive actuator is provided by a precision

Fig. 2 Experimental characterization of the rate-dependent hysteresis loops for the magnetostrictive actuator: **a** Experimental setup; **b** CAD model of the actuator cross section; **c** Measured rate-dependent hystereses; and **d** Estimated magnitude-frequency response with 99.7% significance confidence
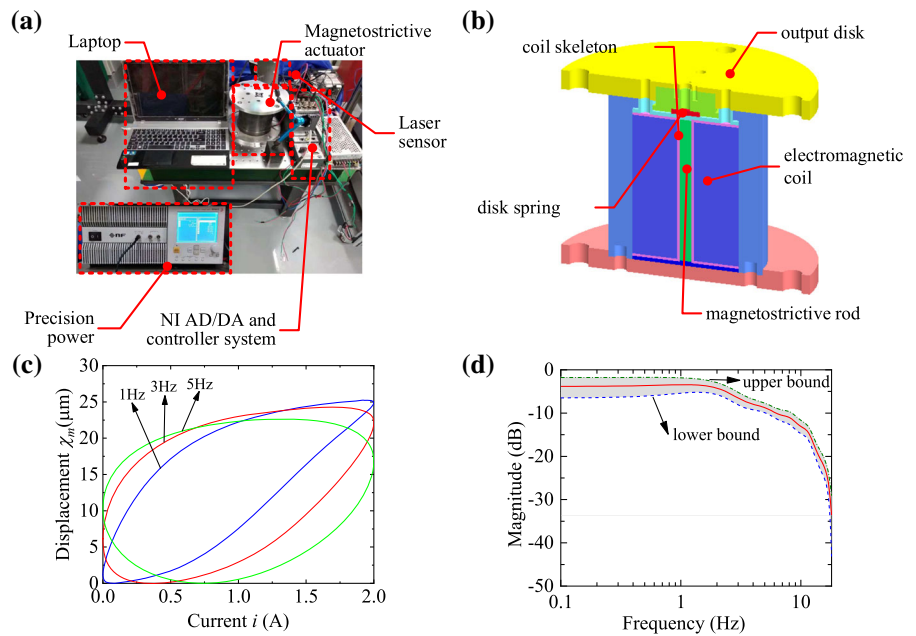
Fig. 3 Experimental characterization of rate-dependent hysteresis loops for the piezoelectric actuator: **a** Experimental setup; **b** CAD model of the piezoelectric actuator; **c** Measured rate dependent hystereses; and **d** Estimated magnitude-frequency response with 99.7% significance confidence.
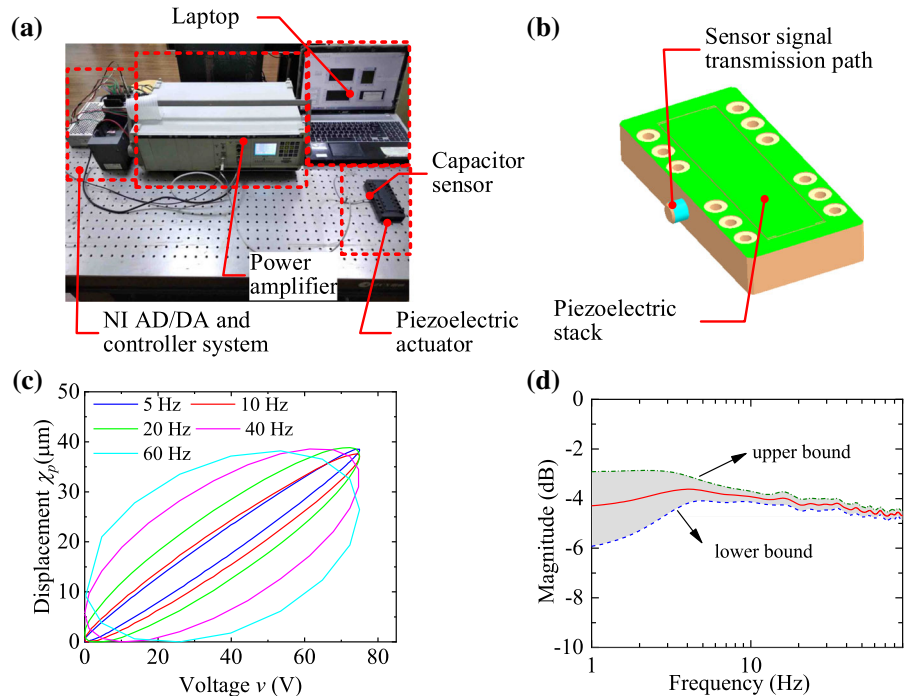
Table 1 Specifications of the magnetostrictive and piezoelectric actuators

Item	Magnetostrictive	Piezoelectric
Device dimension	$\Phi210$ mm$\times$160 mm	132 mm$\times$60 mm$\times$22 mm
Maximum current	3 A	150 V
Maximum displacement	37 μm	75 μm
Displacement resolution	10 nm	1.5 nm
Maximum payload	40 kg	10 kg

power (BP4610, NF Corporation). The NI AD/DA and controller system contain the real-time analog–digital (AD, NI 9263, National Instruments, Inc.), digital–analog (DA, NI 9234, National Instruments, Inc.) and control chassis (CompactRIO 9082, National Instruments, Inc.). The system is deployed for measurement and real-time identification. The hysteresis identification results are visualized in the laptop via the high-speed Ethernet communication between the laptop and CompactRIO 9082 controller. The cross section of the CAD model for magnetostrictive actuator is depicted in Fig. 2b.

The output vs. input loops of the magnetostrictive actuator are shown in Fig. 2c, when the 2 A currents of different frequencies are utilized to drive the magnetostrictive actuator. It is seen that as the input frequencies raise, the loop relative widths increase and the maximum displacements of the magnetostrictive actuator decrease. The rate-dependent effect of the hysteresis can be also reflected by the frequency spectrum graph. A small amplitude of white noise is applied to drive the magnetostrictive actuator for frequency response estimation. Due to the system uncertainty, the estimated frequency response cannot completely match the actual ones of the magnetostrictive actuator. Figure 2d the magnetostrictive magnitude-frequency response with the confidence region of 3σ standard deviation, within the frequency bandwidth [0.1, 20] Hz. The uncertainty band of low frequency is wider than that of high frequency. It is noted that the rate-dependent offline model, e.g., the conventional transfer function, cannot characterize this uncertainty. This statement will be verified in Sec.4.

As shown in Fig. 3a, the capacitor sensor is installed to measure the displacement of the piezoelectric actuator. The measurement and identification hardware are same to those in the magnetostrictive experimental system. The driving voltage of the piezoelectric actuator is supplied by a high-voltage power amplifier (XE-500, Harbin Core Tomorrow Science and Technology Co., Ltd.). The CAD model of the piezoelectric actuator is shown in Fig. 3b.

The output vs. input loops of the piezoelectric actuator are comparatively drawn in Fig. 3c, when the voltages with 75 V and different frequencies are utilized to drive the piezoelectric actuator. Similar to the results of the magnetostrictive actuator, it is seen that the loop widths of the piezoelectric actuator grow intensively with the increasing frequencies, and the symmetry of those loops is better than the magnetostrictive actuator. Figure 3d shows the piezoelectric magnitude-frequency response with the confidence region of 3σ standard deviation, within the frequency bandwidth [1, 90] Hz. Like the magnetostrictive actuator, the rate-dependent part in piezoelectric offline model cannot characterize the frequency spectrum uncertainty.

2.3 Time-varying dynamics for the load/temperature-dependent hysteresis

When the external load on the actuator changes rapidly, or the ambient temperature around the actuator varies slowly, the actuator dynamics changes.

Their effects on the hysteresis loops of the magnetostrictive actuator will be investigated independently according to the experiments.

To describe the load-dependent characteristics of the magnetostrictive hysteresis, a 10 kg weight (envelop is 210 mm $\times$ 100 mm $\times$ 120 mm) is placed onto the magnetostrictive actuator with 4 Hz and 2.5 A Ap-p sinusoidal input current. Figure 4a shows the actuator displacement variation when the load is applied around between 1 s and 3 s. Since the load collides the output disk of the magnetostrictive actuator two times (front first and back second) when placed, there are two disturbances in the displacement curve. Figure 4(b) shows the hysteresis loop variations with the 10 kg external load. At the moment when the load changes, the hysteresis loops oscillate up and down. After the load is stably placed on the output disk of the magnetostrictive actuator, the hysteresis loop is formed in a new equilibrium state. The position and shape of the loop have changed compared with those of the unloaded state.

Fig. 4 Experimental characterization of the load-dependent hysteresis loops for magnetostrictive actuator when a 10 kg load is installed on the actuator output disk: **a** Time series of current and displacement and **b** Load-dependent hysteresis
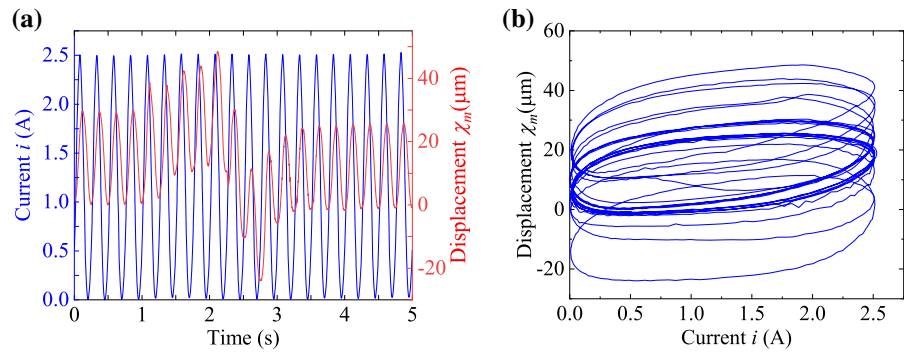
Table 2 Specifications of the magnetostrictive micropositioner

Item	Value
Device dimension	400mm × 120mm × 60mm
Maximum current	3 A
Maximum displacement	340 μ m
Displacement resolution	100 nm
Amplification ratio	12

Another custom-developed magnetostrictive micropositioner (see Fig. 5a) is utilized to examine the temperature-dependent characteristics of the hysteresis loops. The stroke of the magnetostrictive actuator is magnified by an amplified structure which is essentially a lever arm. The specifications of the magnetostrictive micropositioner are illustrated in Table 2. The reason we use this magnetostrictive micropositioner is that its diameter is smaller than the one in Fig. 2a, making it easier to measure the temperature of the actuator housing and thus evaluate heat changes inside the actuator.

The operation of the magnetostrictive micropositioner is affected by the temperature variation. When the surrounding temperature of the magnetostrictive material rises, additional thermal-induced strain is produced, and vice versa. The experimental procedures to study the temperature-dependent characteristics of the hysteresis loops are described as follows: (i) The initial heat is acquired, after a short time of 5 A DC current is applied to the excitation coil of the magnetostrictive actuator; (ii) then the magnetostrictive actuator cools naturally without input current, while the temperature on a surface spot of the magnetostrictive actuator is measured with a radiation infrared thermometer. It is noted that the actual temperature inside the magnetostrictive actuator is higher than the measured.

Figure 5b shows the measured and fitting curves of the temperature vs. time and displacement vs. time, respectively. The displacement is a relative quantity of which the initial value is set to a certain value. From Fig. 5b, it can be seen that the displacement of the magnetostrictive micropositioner decreases as the surrounding temperature declines. The exact displacement vs. temperature model is not discussed because it is out of scope for this work. Next, the 6 Hz sinusoidal motion experiments of the magnetostrictive micropositioner are conducted. Similarly, the initial temperature is obtained by providing a short time of DC current to the excitation coil. During the experiment, the measured temperatures are 42.5 °C at initial time, 38.6 °C at 4 min and 30.4 °C at 14 min. From Fig. 5c, we see that the displacement of the micropositioner decreases from 200 mm to 125 mm when the temperature drops. The corresponding hysteresis loops vary in terms of the shapes and orientations, as shown in Fig. 5d.
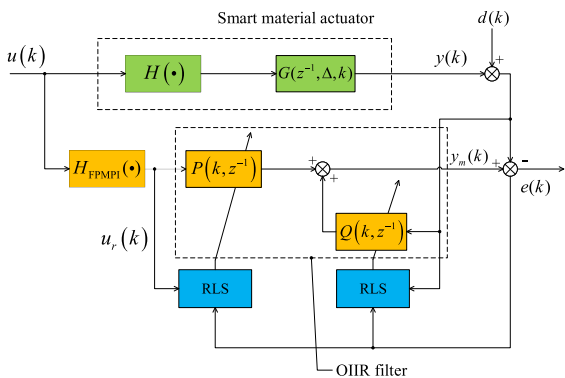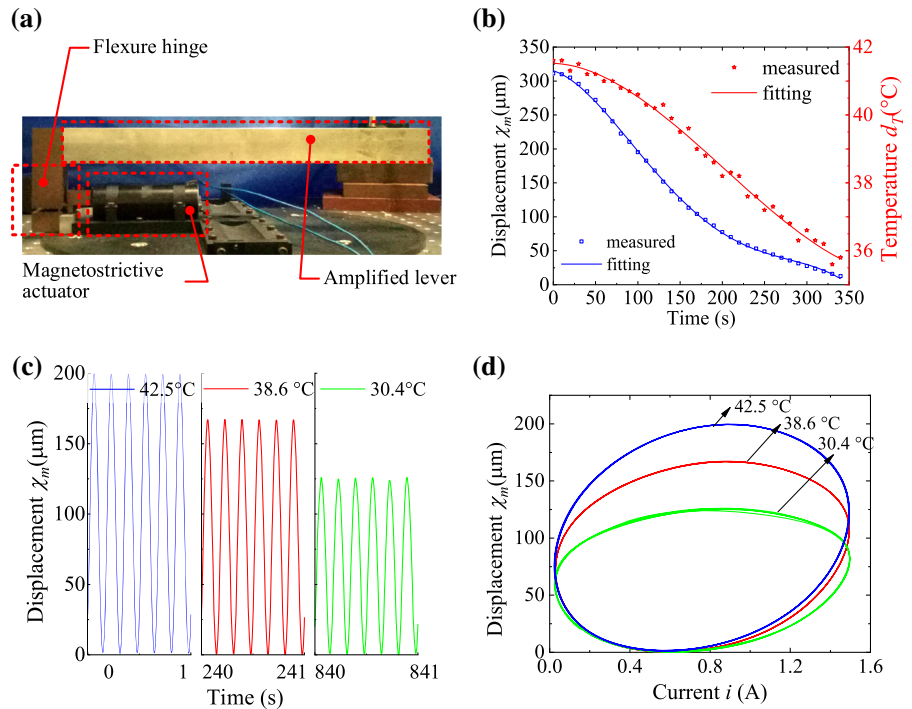
3 Hysteresis online identification approach

To improve the rate/load/temperature-dependent hysteresis modeling accuracy, a hysteresis online identification approach is presented, which will be demonstrated in this section.

The block diagram of the proposed hysteresis online identification approach is shown in Fig. 6. First, the rate-independent nonlinear part $H(\cdot)$ is modeled via the FPMPI model; thus, the input is redefined to u_r and the system can be regarded as linear. Then, the linear dynamics is modeled with the OIIR filter whose parameters are estimated by the adaptive RLS algorithm.

Adaptive online identification is an excellent system modeling strategy to deal with system uncertainty and external disturbance [33–35]. Compared against

Fig. 5 Experimental characterization of the temperature-dependent hysteresis loops for the magnetostrictive micropositioner: **a** Experimental setup; **b** Measured and fitting displacement vs. time and temperature vs. time, respectively; **c** Output displacements with 6 Hz input currents under different surrounding temperatures; and **d** Temperature-dependent hysteresis loops

(a)

(b)

(c)

(d)

Fig. 6 Block diagram of hysteresis online modeling approach for the smart material actuators

the hysteresis offline approach, the dynamic feedback is introduced into system identification process. The main feature of the adaptive identifier is that it achieves the identification objective despite arbitrarily small uncertainty and time variation associated with Δ and $G(z^{-1}, k)$, respectively. In this paper, we assume that the system uncertainty and time-varying dynamics exist in the linear dynamics of the smart material actuator. The phenomena can be described by the OIIR filter.

3.1 Fractional-order polynomial-modified Prandtl–Ishlinskii model

Different from the integer-order polynomial-modified PI model in [2,11,12], in this article, we utilize the fractional-order polynomials to modify the basic PI model, aiming at improving the modeling accuracy of asymmetry and saturate rate-independent hysteresis.

The FPMPI model $H_{\text{FPMPI}}(\cdot)$, shown in Fig. 7a, is utilized to describe the rate-independent hysteresis. The FPMPI model is the cascade of the weighted fractional-order polynomials superposition and weighted Play operators superposition.

The basic PI model is shown in the right part of Fig. 7a. Since the displacements of the magnetostrictive and piezoelectric actuators cover positive range, the single-side Play operator is used in this article. Its discrete form, at time instant k, can be expressed as

$$H_{r_H}[v](k) = \begin{cases} \max\{v(k) - r_H, \min\{v(k), H_{r_H}[v](k-1)\}\}; & k \geqslant 1 \\ \max\{v(0) - r_H, \min\{v(0), H_{r_H}[v](0)\}\}; & k = 0 \end{cases}$$

$$(1)$$

where v and H_{r_H} are the input and output of the Play operator, respectively, $H_{r_H}[0]$ is the initial value which is often set to 0, and r_H is the threshold value of Play operator. PI model is formulated with the weighted Play

Fig. 7 FPMPI model to describe the asymmetric and saturate rate-independent hysteresis: **a** Structure of the FPMPI model; **b** Elementary fractional-order polynomial function; and **c** Comparison of the FPMPI (the elementary polynomial vector is $[1, u, u^2, u^{1/2}]$) and IPMPI models (the elementary polynomial vector is $[1, u, u^2, u^3]$)
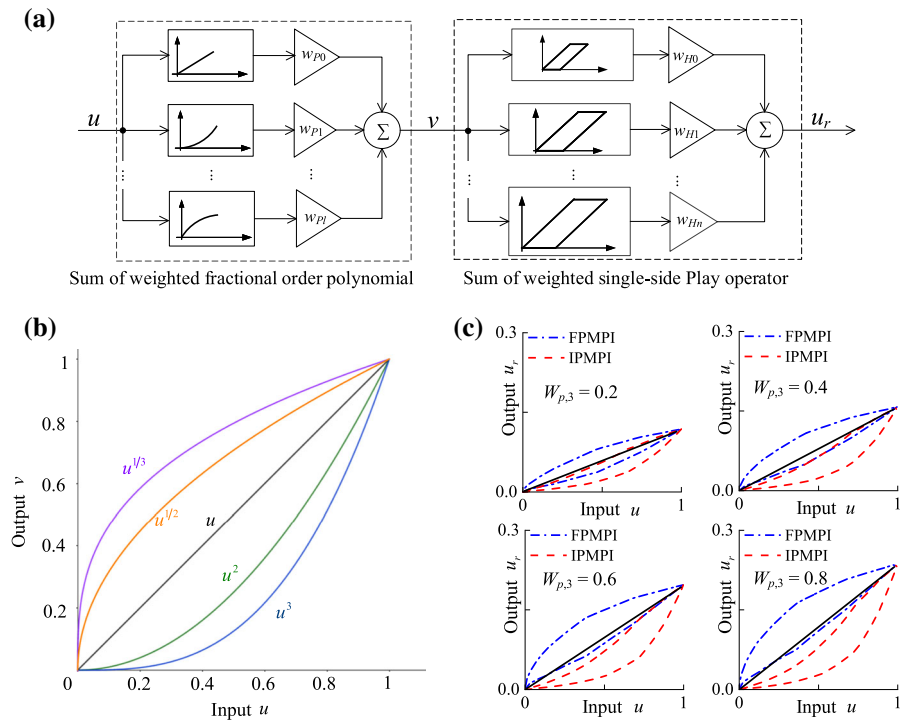
operator superposition as

$$H[v](k) = \boldsymbol{H}_{r_H}[v](k) \cdot \boldsymbol{w}_H^{\mathrm{T}} \tag{2}$$

where $\boldsymbol{H}_{r_H} = [H_{r_H,0}, H_{r_H,1}, \cdots, H_{r_H,N}]$ is the Play operator vector, and $\boldsymbol{w}_H = [w_{H,0}, w_{H,1}, \cdots, w_{H,N}]$ is the weight vector.

$\boldsymbol{r}_H = [r_{H,0}, r_{H,1}, \cdots, r_{H,1}, \cdots, r_{H,N}]$ is the threshold vector corresponding to the Play operator vector, and its $(i+1)^{\mathrm{th}}$ element is given by

$$r_{H,i} = \frac{i}{N+1} \max\{|v(k)|\}; \quad i = 0, 1, 2, \cdots, N. \tag{3}$$

Before the PI model, the input u is propagated to the sum of weighted fractional-order polynomial. The overall system is called fractional-order polynomial-modified PI model, and its mathematical formulation is given as

$$u_r(k) = H[u](k) = \boldsymbol{H}_{r_H}[\boldsymbol{P}[u] \cdot \boldsymbol{w}_P^T](k) \cdot \boldsymbol{w}_H^T \tag{4}$$

where $u_r(k)$ is the FPMPI model output, $\boldsymbol{H}$ is the FPMPI model, $\boldsymbol{P} = [p_0, p_1, \cdots, p_i, \cdots, p_L]$ is the fractional polynomial operator vector whose dimension is $L+1$ (L is an odd number), and its $(i+1)^{\mathrm{th}}$ ($i = 0, 1, 2, \cdots, L$) element is given by

$$p_i = \begin{cases} u^i; & i = 0, 1 \\ u^{\frac{i}{2}+1}; & i = 2, 4, 6, \cdots, L-1 \\ u^{\frac{2}{i+1}}; & i = 3, 5, 7, \cdots, L. \end{cases} \tag{5}$$

where $\boldsymbol{w}_P = [w_{P,0}, w_{P,1}, \cdots, w_{P,L}]$ is the weight vector of the fractional polynomial operator.

The graphs of the elementary fractional-order polynomial functions are shown in Fig. 7b, where the function inputs and outputs are normalized to interval [0, 1]. It is seen that $u^{1/2}$ and $u^{1/3}$ are symmetric to u^2 and u^3 along the line $y = u$, respectively. It can be predicted that with the combination of the weighted fractional-order polynomials, the modified PI model will be more capable of describing the asymmetric and saturate hysteresis compared with the pure integer-order polynomials.

Next, we will use a simulation example to compare the difference between the integer-order and fractional-order polynomial-modified PI models in describing the asymmetry and saturate hysteresis loop. In Eq. (4), $\boldsymbol{P}[u]$s are set to $[1, u, u^2, u^{1/2}]$ and $[1, u, u^2, u^3]$ for FPMPI and IPMPI models, respectively; $\boldsymbol{w}_P$ and $\boldsymbol{w}_H$ are set to $[0, 0.3, 0.1, w_{P,3}]$ and $[0.1, 0.05, 0.1, 0.04]$, respectively. The weights $\boldsymbol{w}_P$ and $\boldsymbol{w}_H$ of FPMPI and IPMPI differ in the weight values of $u^{1/2}$ and u^3. When the value of $w_{P,3}$ increases from 0 and 1, the hysteresis loops constructed by FPMPI are more close to the asymmetric saturation hysteresis loops of the magnetostrictive actuator (see in Fig. 2c) by the contrast with the IPMPI. It can be illustrated from the simulation

results (Fig. 7c) where $w_{P,3} = 0.2, 0.4, 0.6, 0.8$, the reason is that the integer- and non-integer-order polynomials of the FPMPI model are located on either side of the line $u_r = u$, and the actual hysteresis curve can be described more accurately based on the different weights of the FPMPI model.

3.2 Rate-dependent subsystem online identification

The dynamics of the smart material actuators are constructed by the OIIR filters. The structure of the OIIR model is shown as

$$\hat{G}(z^{-1}, k) = \frac{Y_m(z^{-1}, k)}{U_r(z^{-1}, k)} = \frac{P(z^{-1}, k)}{1 - Q(z^{-1}, k)} \qquad (6)$$

where $Y_m(z^{-1}, k)$ and $U_r(z^{-1}, k)$ are the Z-transforms of the output and input of the actuator dynamics, respectively; $P(z^{-1}, k) = \sum_{i=0}^{M} p_i(k)z^{-i}$, $Q(z^{-1}, k) = \sum_{j=1}^{N} q_j(k)z^{-j}$; $p_i(k)$ and $q_j(k)$ are the time-variant numerator and denominator coefficients of the OIIR filter—these coefficients are also called OIIR filter weights; $M+1$ and $N+1$ are the numerator and denominator orders of the OIIR filter.

In terms of the conventional IIR-based system identification method, the output error $e(k)$ is formulated as follows:

$$e(k) = y(k) - \boldsymbol{w}(k)\boldsymbol{\varphi}(k) \qquad (7)$$

where

$$\boldsymbol{\varphi}(k) = [u_r(k), \cdots, u_r(k - M), y_m(k - 1), \cdots, \\ y_m(k - N)]^T \qquad (8)$$

is the input signal sequence satisfying the persistent excitation condition;

$$\boldsymbol{w}(k) = [p_0(k), \cdots, p_M(k), q_1(k), \cdots, q_N(k)] \qquad (9)$$

is the weight vector of the OIIR filter; and y is the actual output of the actuator.

According to Eq. (7), the feedback signal that transmits to $Q(z^{-1})$ is the OIIR filter output signal $y_m(k)$. Under this condition, the error evaluation function, by which the optimal weight coefficients of the IIR-based dynamics are acquired, may be non-quadratic. Consequently, the local minimum estimation error may be obtained [36]. To overcome this drawback, the actual output signal $y(k)$ is used to replace the model output signal $y_m(k)$ to determine the weight coefficients

of $Q(z^{-1})$, as shown in Fig. 6. Therefore, the modified error $\bar{e}(k)$ is formulated as

$$\bar{e}(k) = y(k) - \boldsymbol{w}^T(k)\bar{\boldsymbol{\varphi}}(k) \qquad (10)$$

where

$$\bar{\boldsymbol{\varphi}}(k) = [u_r(k), \cdots, u_r(k - M), y(k - 1), \cdots, \\ y(k - N)]^T. \qquad (11)$$

Note that $e(k)$ is called "equation error" in Eq. (7), as against the "output error" $\bar{e}(k)$ in Eq. (10).

The weight vector $\boldsymbol{w}(k)$ is estimated by minimizing the least-square error $\xi(n)$ at time instant n as

$$\min \xi(n) = \sum_{i=0}^{n} \lambda^{n-i} \bar{e}^2(i). \qquad (12)$$

where λ $(0 < \lambda \leqslant 1)$ is the "forgetting factor" that makes the older error sequences exert less influence upon the optimization process.

This minimization problem can be solved by the recursive least squares (RLS) technique, and the weight auto-tuning process is given as

$$\boldsymbol{P}(n+1) = \frac{1}{\lambda}\left[\boldsymbol{P}(n) - \frac{\boldsymbol{P}(n)\bar{\boldsymbol{\varphi}}(n)\bar{\boldsymbol{\varphi}}^T(n)\boldsymbol{P}(n)}{\lambda + \bar{\boldsymbol{\varphi}}^T(n)\boldsymbol{P}(n)\bar{\boldsymbol{\varphi}}(n)} \right] \qquad (13)$$

$$\boldsymbol{w}^T(n+1) = \boldsymbol{w}^T(n) + \boldsymbol{P}(n+1)\bar{\boldsymbol{\varphi}}\bar{e}(n).$$

where $\boldsymbol{P}(n)$ is the inverse of the correlation matrix $\boldsymbol{R}(n)$ of the input sequence $\boldsymbol{u}_r(n)$. The initial value of matrix $\boldsymbol{P}(n)$ is set to the inverse of the input signal power estimate. The K-dimension $(K = M + N + 1)$ squared matrix $\boldsymbol{R}(n)$ is formulated as

$$\begin{bmatrix} r(0) & r(1) & \ldots r(K-1) \\ r(-1) & r(0) & \ldots r(K-2) \\ r(-2) & r(-1) & \ldots r(K-3) \\ \vdots & \vdots & \ddots & \vdots \\ r(-K+1) & r(-K+2) & \ldots & r(0) \end{bmatrix} \qquad (14)$$

where $r(k)$ is the autocorrelation function of the input sequence $\boldsymbol{u}_r(n)$ at lag k.

Compared Fig. 1 with Fig. 6, it is observed that the system uncertainty Δ and external disturbance $d(k)$ can not be modeled for the hysteresis offline identification approach. However, their effect upon system model is considered in the OIIR filter—Δ and $d(k)$ are introduced into the online identification algorithm and reflected by the time-variant weight coefficients of the OIIR filter.

4 Hysteresis identification results and discussion

With the experimental setups shown in Fig. 2a, Fig. 3a and Fig. 5a, the rate/load/temperature-dependent hysteresis online identification experiments are conducted. Meanwhile, the hysteresis offline identification results for the smart material actuators will be compared to the online results.

4.1 Magnetostrictive hysteresis identification results

The measured current and displacement are normalized to 3 A and 37 μ m, respectively, that is, normalized current $\bar{i}$ and displacement $\bar{\chi}_m$, respectively.

To identify the rate-independent hysteresis, the 0.05 Hz sinusoidal currents of which the amplitudes increase arithmetically from 0.3 A to 3 A are applied to drive the magnetostrictive actuator. With the measured input/output data and FPMPI model in Eq. (4), the weight coefficients of Play and fractional-order polynomial operators, w_H and w_P, are obtained, as shown in Table 3. The orders of w_H and w_P are set 10 and 8, respectively, with the trade-off between identification accuracy (more than 97%) and computational complexity (to keep low). Based on the acquired FPMPI model and particle swarm optimization algorithm command *particleswarm* in MATLAB, we compare the identified rate-dependent hysteresis against the actual as depicted in Fig. 8a. It is seen that although there exists certain identification error in some regions, the FPMPI model totally describes the asymmetric and saturate rate-dependent hysteresis well—the relative identified error is 2.83% in RMS sense.

As for the hysteresis offline identification approach, transfer function-based dynamics of the magnetostrictive actuator are obtained offline. A small amplitude 0.1–20 Hz band-limited current is utilized to drive the actuator. As shown in Fig. 1, with the intermediate signal u_r and output displacement y, the parameters of the transfer function are estimated offline by *tfest* in MATLAB. To keep relatively low computation complexity and small identification error ($<3\%$), the numerator and denominator orders of the transfer function are selected as 8 and 4, and the delay constant is set to 1 with trial and error. The specified structure of the transfer function is formulated as

$$\hat{G}(z^{-1}) = z^{-d} \frac{\sum_{j=1}^{J} b_j z^{-i}}{1 + \sum_{i=1}^{I} a_i z^{-i}} \tag{15}$$

Table 3 Weight coefficients of the offline-identified rate-independent hysteresis for the magnetostrictive actuator

Order	w_H	w_P
1	0.3955	0.0057
2	0.2042	0.4640
3	0.4940	0.2343
4	0.3927	−1.0113
5	0.7198	0.5568
6	0.1228	0.7493
7	0.1889	−0.9740
8	0.1550	0.4889
9	0.2058	–
10	−0.0060	–

where $d = 1$, $a_i(i = 1 \cdots I, I = 9)$ and $b_j(j = 1 \cdots J, J = 4)$ are the elements of the coefficient vectors

$$\boldsymbol{a} = [0, 1.90, -10.00, 21.05, -22.16,$$
$$11.65, -2.44, 0.016, -0.016]^{\mathrm{T}} \tag{16}$$

and

$$\boldsymbol{b} = [-3.64, 4.95, -2.99, 0.67]^{\mathrm{T}} \tag{17}$$

, respectively.

The dynamics identification results of magnetostrictive actuator are shown in Fig. 8b, where the actual frequency response curve is obtained by *tfestimate* in MATLAB.

It can be seen that the actual and transfer function identified frequency response curves match fairly well. The dynamics identification accuracies of the magnetostrictive actuator vary at different frequencies—at some frequencies, the identification accuracies deteriorate. It is noted that the transfer function identified dynamics will result in great errors if there exists system uncertainty as shown in Fig. 2d.

Differing from the hysteresis offline identification approach, the OIIR filter-based dynamics is acquired in real time. The actual current and displacement of the magnetostrictive actuator are detected at every sampling time via CompactRIO 9082 real-time system. The numerator and denominator orders, M and N, in Eq. (6) are set to 3 and 5, respectively, by the trade-off of accuracy and time cost. The forgetting factor λ in Eq.(12) is set to 1. The initial value of the correlation matrix $\boldsymbol{R}(n)$ in Eq. (13) is set to $10^5 \boldsymbol{I}$. After shorter transient processes (around a few microseconds), the

Fig. 8 Rate-independent hysteresis and dynamics via the offline identification approach: **a** Comparison of the actual and FPMPI identified rate-independent hystereses; **b** Comparison of the actual and transfer function identified dynamics
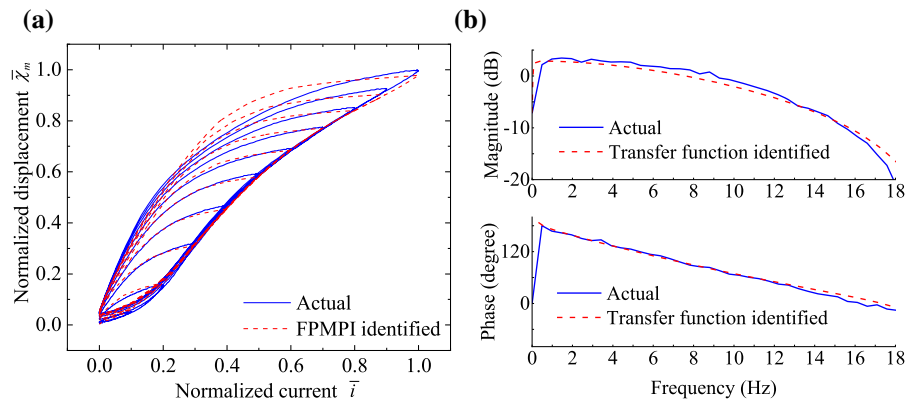
Fig. 9 Comparison of the offline- and online-identified rate-dependent hystereses for **a** 1 Hz and **b** 5 Hz input currents with the cases in Fig. 2
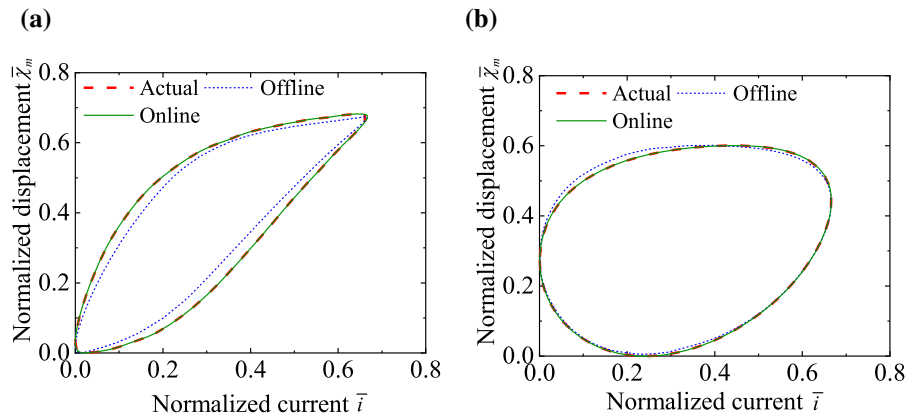

weight vector of the OIIR filter converges quickly to a stable value. Afterward, the online-identified hystereses at steady state are compared against the actual ones.

The offline- and online-identified rate-dependent hystereses of the magnetostrictive actuator are comparatively illustrated in Fig. 9. Figure 9a and b correspond to the cases of 1 Hz and 5 Hz input currents, respectively. It is observed that although the actual hysteresis loop shapes of the magnetostrictive actuator change dramatically, both offline- and online-identified hysteresis loops can adapt to the variation of the actual ones. The relative identification errors of 1 Hz and 5 Hz hystereses are 2.91% and 2.88%, respectively, in RMS sense. However, the uncertainty in smart material actuators is not considered for hysteresis offline identification approach. With the proposed online identification approach, the hysteresis identification accuracy improves because the offline-model uncertainty is characterized by the OIIR.

The hysteresis offline model cannot accurately follow the change of the real hysteresis loop, when the disturbance affects the output of the smart material

actuator. Figure 10a compares the offline- and online-identified load-dependent hysteresis curves. When the load collides with the output disk of the magnetostrictive actuator, the hysteresis curve oscillates. However, the original offline-identified hysteresis curve remains unchanged. As a comparison, the hysteresis online model can accurately follow the change of the real hysteresis loop, in three situations where no external load is applied (before 1 s), the load collides with the actuator (1 s to 3 s), and the load is applied (after 3 s). Fig. 10b compares the offline- and online-identified temperature-dependent hysteresis curves. When the surrounding temperature decreases from 42.5 °C to 30.4 °C, the thermal-induced strain of the magnetostrictive material decreases and the shapes of hysteresis loops change. The offline-identified hysteresis model cannot track this change. As a comparison, it is seen that the actual hystereses with the surrounding temperature 42.5 °C, 38.6 °C and 30.4 °C are described very well with the proposed hysteresis online identification approach.

Fig. 10 **a** Comparison of the offline- and online-identified load-dependent hysteresis with the case in Fig. 4b; **b** Comparison of the offline- and online-identified temperature-dependent hysteresis with the case in Fig. 5d; Time series of the OIIR filter coefficients of the identified **c** Load- and **d** temperature-dependent hystereses, corresponding to the cases of Fig. 4b and Fig. 5d, respectively
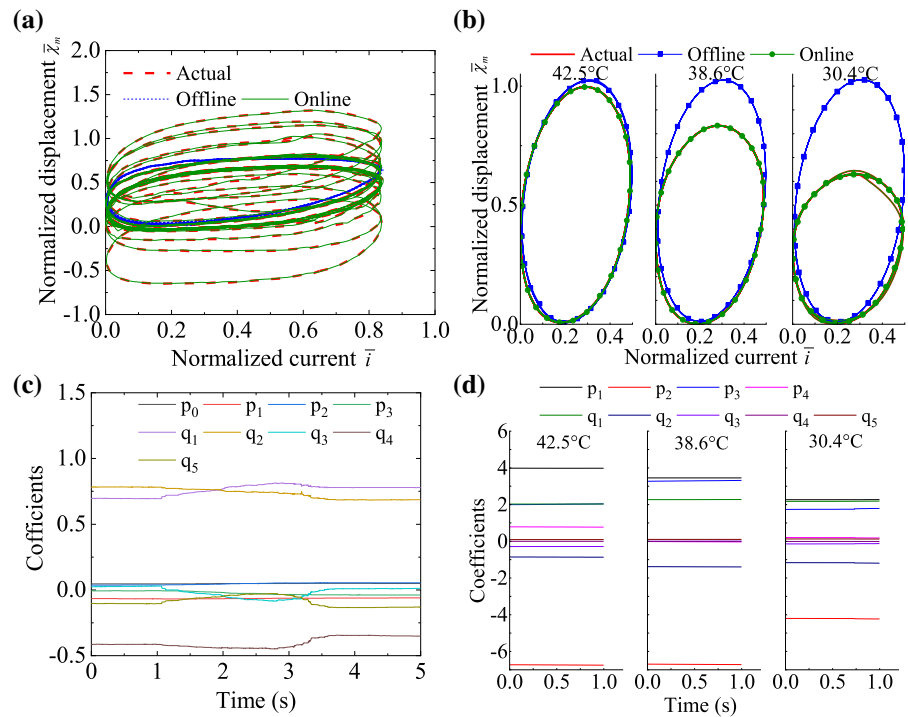
To demonstrate the virtues of the hysteresis online identification approach, the time series of the OIIR filter coefficients, $p_i (i = 0 \cdots 3)$ and $q_i (i = 1 \cdots 5)$ in Eq. (6), are shown in Fig. 10c and d. Although the external load leads to the varying hysteresis loops, the OIIR filter is capable of adjusting its own parameters, so as to track the variation of hysteresis loops (see Fig. 10c). Figure 10d shows the OIIR filter coefficients reduce with the decreasing surrounding temperature, because the output displacements of the magnetostrictive actuator reduce with the decreasing surrounding temperature.

Since the online model is applicable for the system running with variable external disturbance, it can be extended to control position servo drive system of high speed and high precision. Moreover, the hysteresis online model can completely comprehend the dynamics of an evolving complex process. It can accommodate a useful representation of the process model in some situations where the continuous detection of the system states is required.

4.2 Piezoelectric hysteresis online identification results

The measured voltage and displacement are normalized to 150 V and 75 μ m, respectively, that is, normalized voltage $\bar{v}$ and displacement $\bar{\chi}_p$, respectively.

Like the hysteresis offline identification approach for magnetostrictive actuator, the 0.1–100 Hz band-limited current of small amplitude is treated as the input signal to identify the dynamics of the piezoelectric actuator. In order to identify the rate-independent hysteresis, the 0.1 Hz sinusoidal input voltage of which the amplitude increases arithmetically from 15 V to 150 V is applied to drive the piezoelectric actuator. The rate-independent hysteresis and linear invariant dynamics are cascaded to offline identify the rate-dependent hysteresis for piezoelectric actuator. Figure 11 compares the offline- and online-identified hystereses. The rate-dependent hystereses with the sinusoidal (10 Hz, 60 Hz) and triangle (10 Hz, 20 Hz) input voltages of constant amplitude are measured and identified. It is seen that with the offline model, the identified hystereses track the actual accurately despite with the different types of input voltages. There exist larger errors

Fig. 11 Comparison of the offline- and online-identified rate-dependent hystereses with **a** 10 Hz, **b** 60 Hz sinusoidal and **c** 10 Hz, **d** 20 Hz triangle input voltages
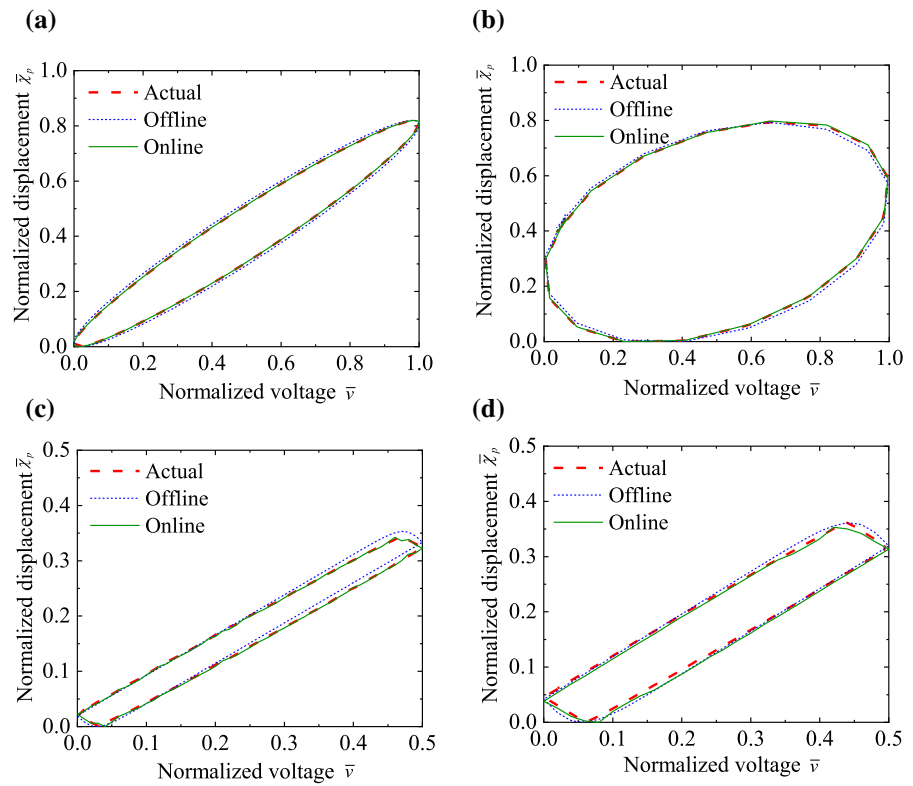
in the corners of hysteresis loop in Fig. 11c and d. The reason is that the derivatives of input triangle signal in those positions are discontinuous, resulting in some oscillation for output signal. However, it is seen that with the proposed hysteresis online identification approach, the actual hystereses can be tracked well by the online-identified ones under the different types of input voltages. Particularly, when the input is 10 Hz and 20 Hz triangle voltages, the online identification errors are reduced obviously by the contrast with the offline.

4.3 Shape memory alloy actuator

In Ref. [37], the ambient temperature and rotation angle of a two-wire SMA actuator are measured. Figure 12a shows the experimental setup of the two-wire SMA actuator. When the amplitudes of the ambient temperature increase slowly from 80 °C to 370 °C, the hysteresis loop varies for the SMA actuator. The measured temperature and rotation angle of the SMA actuator are normalized to 370 °C and 32 degrees, respectively, that is, normalized temperature $\bar{T}$ and rotation angle

$\bar{\chi}_S$, respectively. The experimental data are applied in this paper.

Since the rotation of the SMA actuator shows quasi-static state, the sole FPMPI model is utilized to identify its hysteresis offline. We select the orders of $\boldsymbol{w}_H$ and $\boldsymbol{w}_P$ as 10 and 8. Based on the particle swarm optimization algorithm command *particleswarm* in MATLAB, we compare the offline-identified hysteresis against the actual as depicted in Fig. 12b. Furthermore, based on the iterative hysteresis identification algorithm in Fig. 6, we conduct the real-time simulation for the two-wire SMA actuator hysteresis identification. The online-identified hysteresis is compared against the actual and offline-identified as shown in Fig. 12b. It is seen that the online-identified model describes the actual hysteresis more accurately. Statistical analysis shows that the hysteresis relative modeling errors are 4.23% and 0.10% with the offline and online identification approaches, respectively.

To quantitatively evaluate the hysteresis online identification performance, the relative modeling errors in Norm-2 sense and in Norm-∞ sense, i.e., re$_{N2}$ and

Fig. 12 Hysteresis online identification for SMA actuator: **a** Experimental setup; **b** Comparison of the offline- and online-identified temperature-dependent hystereses

(a)

(b)
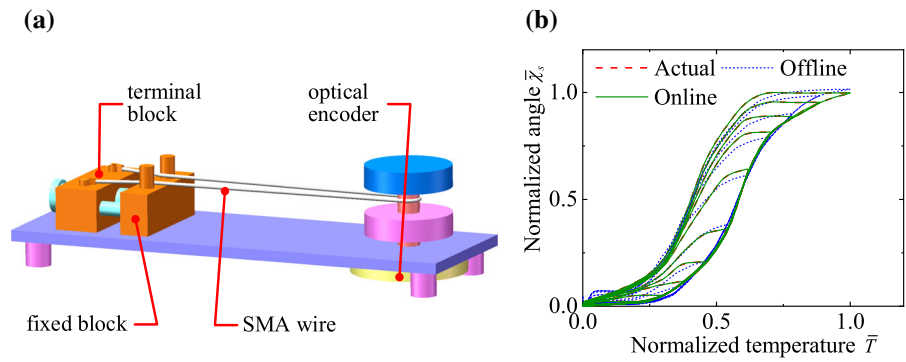
Table 4 Relative identification errors (%) of the rate/load/temperature-dependent hysteresis for the magnetostrictive, piezoelectric and SMA actuators

Magnetostrictive actuator					
Input current	External disturbance	$re_{N2,off}$	$re_{N2,on}$	$re_{N\infty,off}$	$re_{N\infty,on}$
1 Hz sine	No	5.16	0.02	7.31	0.04
5 Hz sine	No	2.29	0.01	3.69	0.02
4 Hz sine	10 kg load	45.03	1.16	60.57	4.50
6 Hz sine	42.5°C	3.43	0.04	3.71	0.10
6 Hz sine	38.6°C	21.06	0.03	23.36	0.04
6 Hz sine	30.4°C	58.12	0.08	65.78	0.66
Piezoelectric actuator					
Input voltage	External disturbance	$re_{N2,off}$	$re_{N2,on}$	$re_{N\infty,off}$	$re_{N\infty,on}$
10 Hz sine	No	1.81	0.10	1.98	0.17
60 Hz sine	No	2.94	0.15	2.68	0.47
10 Hz triangle	No	3.50	0.92	4.25	2.12
20 Hz triangle	No	2.95	1.30	3.69	2.38
SMA actuator					
Input temperature	External disturbance	$re_{N2,off}$	$re_{N2,on}$	$re_{N\infty,off}$	$re_{N\infty,on}$
80–370 °C	No	4.23	0.10	5.82	0.26

$re_{N\infty}$, respectively, are defined by

$$re_{N2} \triangleq \frac{||y - y_m||_2}{||y_a||_2} \times 100\%, \tag{18}$$

$$re_{N\infty} \triangleq \frac{||y - y_m||_\infty}{||y||_\infty} \times 100\%$$

where y and y_m are the waveforms of the actual and identified outputs, respectively. Table 4 comparatively shows the values of re_{N2} and $re_{N\infty}$ for the hysteresis offline and online identification of the magnetostrictive and piezoelectric actuators. The subscripts, "off" and "on," represent the offline- and online-identified hystereses, respectively. From Table 4, it is cogently concluded that with the proposed hysteresis online identi-

fication approach, the rate/load/temperature-dependent hysteresis of the smart material actuators can be described much better than the offline approach.

By summarizing the hysteresis online identification results of three types of smart material actuators, it can be concluded that the hysteresis online model can characterize the uncertainty of the offline model. As such, the online model-based controller is much potential to apply in the ultra-precision position and attitude tracking control system.

It is necessary to point out that comparison of the offline and online identification techniques reveals that additional detection and information processing

equipment are required for online identification. More importantly, it necessitates sensors of high data transfer performance and processors of high operational speed. Nevertheless, with the development of intelligent and integrated electronic devices, the aforementioned drawbacks of the hysteresis online identification methodology will be overcome.

5 Conclusion

In this article, we report a FPMPI and OIIR integrated model to online identify the rate/load/temperature-dependent hystereses for the magnetostrictive, piezoelectric and shape memory actuators. The custom-developed magnetostrictive, commercial piezoelectric and existing SMA actuators are employed to verify the proposed hysteresis online identification approach. First of all, the traditional Hammerstein-based hysteresis offline identification approach is introduced. The Hammerstein-based model incorporates a PMPI and transfer function sub-models. However, due to the system uncertainty, the rate-dependent hysteresis cannot be modeled accurately via the offline identification approach. Moreover, the offline-modeled hysteresis cannot track the actual varying hysteresis with the external load and temperature, respectively. Then, instead of the offline transfer function, we apply an OIIR filter to capture system uncertainty and time-varying dynamics. According to the experimental result comparison between the offline and online approaches, it is found that all hysteresis online identification results are better significantly than the offline ones with different input signals and external disturbances. In the future, we will further develop the hysteresis online identification approach by constructing an online FPMPI model to improve modeling accuracy and robust ability.

Declarations

Conflict of interest The authors have not disclosed any competing interests.

References

1. Zhang, H.T., Hu, B., Li, L., Chen, Z., Wu, D., Xu, B., Huang, X., Gu, G., Yuan, Y.: Distributed hammerstein modeling for cross-coupling effect of multiaxis piezoelectric micropositioning stages. IEEE/ASME Trans. Mechatron. **23**(6), 2794 (2018)
2. Yi, S., Yang, B., Meng, G.: Microvibration isolation by adaptive feedforward control with asymmetric hysteresis compensation. Mech. Syst. Signal Process. **114**, 644 (2019)
3. Al Janaideh, M., Al Saaideh, M., Rakotondrabe, M.: On hysteresis modeling of a piezoelectric precise positioning system under variable temperature. Mech. Syst. Signal Process. **145**, 106880 (2020)
4. Meng, A., Yang, J., Li, M., Jiang, S.: Research on hysteresis compensation control of gmm. Nonlinear Dyn. **83**(1–2), 161 (2016)
5. Li, Z., Shan, J.: Modeling and inverse compensation for coupled hysteresis in piezo-actuated fabry-perot spectrometer. IEEE/ASME Trans. Mechatron. **22**(4), 1903 (2017)
6. Fleming, A.J., Yong, Y.K.: An ultrathin monolithic xy nanopositioning stage constructed from a single sheet of piezoelectric material. IEEE/ASME Trans. Mechatron. **22**(6), 2611 (2017)
7. Al Janaideh, M., Rakotondrabe, M.: Precision motion control of a piezoelectric cantilever positioning system with rate-dependent hysteresis nonlinearities. Nonlinear Dyn. **65**, 1–21 (2021)
8. Li, Z., Shan, J., Gabbert, U.: Inverse compensation of hysteresis using krasnoselskii-pokrovskii model. IEEE/ASME Trans. Mechatron. **23**(2), 966 (2018)
9. Fang, L., Wang, J., Zhang, Q.: Identification of extended hammerstein systems with hysteresis-type input nonlinearities described by preisach model. Nonlinear Dyn. **79**(2), 1257 (2015)
10. Rakotondrabe, M.: Multivariable classical prandtl-ishlinskii hysteresis modeling and compensation and sensorless control of a nonlinear 2-dof piezoactuator. Nonlinear Dyn. **89**(1), 481 (2017)
11. Qin, Y., Tian, Y., Zhang, D., Shirinzadeh, B., Fatikow, S.: A novel direct inverse modeling approach for hysteresis compensation of piezoelectric actuator in feedforward applications. IEEE/ASME Trans. Mechatron. **18**(3), 981 (2013)
12. Yi, S., Yang, B., Meng, G.: Ill-conditioned dynamic hysteresis compensation for a low-frequency magnetostrictive vibration shaker. Nonlinear Dyn. **96**(1), 535 (2019)
13. Al Janaideh, M., Aljanaideh, O.: Further results on open-loop compensation of rate-dependent hysteresis in a magnetostrictive actuator with the prandtl-ishlinskii model. Mech. Syst. Signal Process. **104**, 835 (2018)

14. Drinčić, B., Tan, X., Bernstein, D.S.: Why are some hysteresis loops shaped like a butterfly? Automatica **47**(12), 2658 (2011)

15. Xiao, S., Li, Y.: Modeling and high dynamic compensating the rate-dependent hysteresis of piezoelectric actuators via a novel modified inverse preisach model. IEEE Trans. Control Syst. Technol. **21**(5), 1549 (2013)

16. Aljanaideh, O., Al Janaideh, M., Rakheja, S., Su, C.Y.: Compensation of rate-dependent hysteresis nonlinearities in a magnetostrictive actuator using an inverse prandtl-ishlinskii model. Smart Mater. Struct. **22**(2), 025027 (2013)

17. Aljanaideh, O., Rakheja, S., Su, C.Y.: Experimental characterization and modeling of rate-dependent asymmetric hysteresis of magnetostrictive actuators. Smart Mater. Struct. **23**(3), 035002 (2014)

18. Wong, P.K., Xu, Q., Vong, C.M., Wong, H.C.: Rate-dependent hysteresis modeling and control of a piezostage using online support vector machine and relevance vector machine. IEEE Trans. Indus. Electron. **59**(4), 1988 (2011)

19. Zhang, D., Jia, M., Liu, Y., Ren, Z., Koh, C.S.: Comprehensive improvement of temperature-dependent jiles-atherton model utilizing variable model parameters. IEEE Trans. Magnet. **54**(3), 1 (2017)

20. Li, P., Yan, F., Ge, C., Wang, X., Xu, L., Guo, J., Li, P.: A simple fuzzy system for modelling of both rate-independent and rate-dependent hysteresis in piezoelectric actuators. Mech. Syst. Signal Process. **36**(1), 182 (2013)

21. Tan, X., Baras, J.S.: Modeling and control of hysteresis in magnetostrictive actuators. Automatica **40**(9), 1469 (2004)

22. Zhang, X., Tan, Y., Su, M., Xie, Y.: Neural networks based identification and compensation of rate-dependent hysteresis in piezoelectric actuators. Phys. B: Condensed Matter **405**(12), 2687 (2010)

23. Davino, D., Giustiniani, A., Visone, C.: Design and test of a stress-dependent compensator for magnetostrictive actuators. IEEE Trans. Magnet. **46**(2), 646 (2010)

24. Zhang, Z., Mao, J., Zhou, K.: Experimental characterization and modeling of stress-dependent hysteresis of a giant magnetostrictive actuator. Sci. China Technol. Sci. **56**(3), 656 (2013)

25. Zhan, Y.S., Lin, C.H.: A constitutive model of coupled magneto-thermo-mechanical hysteresis behavior for giant magnetostrictive materials. Mech. Mater. **148**, 103477 (2020)

26. Valadkhan, S., Morris, K., Shum, A.: A new load-dependent hysteresis model for magnetostrictive materials. Smart Mater. Struct. **19**(12), 125003 (2010)

27. Nouicer, A., Nouicer, E., Mahtali, M., Feliachi, M.: A neural network modeling of stress behavior in nonlinear magnetostrictive materials. J. Superconductivity Novel Magnet. **26**(5), 1489 (2013)

28. Li, Z., Zhang, X., Gu, G.Y., Chen, X., Su, C.Y.: A comprehensive dynamic model for magnetostrictive actuators considering different input frequencies with mechanical loads. IEEE Trans. Indus. Inf. **12**(3), 980 (2016)

29. Hsu, J.T., Ngo, K.D.: A hammerstein-based dynamic model for hysteresis phenomenon. IEEE Trans. Power Electron. **12**(3), 406 (1997)

30. Köhler, R., Rinderknecht, S.: A phenomenological approach to temperature dependent piezo stack actuator modeling. Sensors Actuat. A: Phys. **200**, 123 (2013)

31. Wang, T.Z., Zhou, Y.H.: Nonlinear dynamic model with multi-fields coupling effects for giant magnetostrictive actuators. Int. J. Solids Struct. **50**(19), 2970 (2013)

32. Bhadriraju, B., Narasingam, A., Kwon, J.S.I.: Machine learning-based adaptive model identification of systems: Application to a chemical process. Chem. Eng. Res. Des. **152**, 372 (2019)

33. Yang, C., Jiang, Y., He, W., Na, J., Li, Z., Xu, B.: Adaptive parameter estimation and control design for robot manipulators with finite-time convergence. IEEE Trans. Indus. Electron. **65**(10), 8112 (2018)

34. Su, L., Huang, X., Song, M.I., LaFave, J.M.: Structures. Elsevier, Amsterdam (2020)

35. Lu, W., Tang, B., Ji, K., Lu, K., Wang, D., Yu, Z.: A new load adaptive identification method based on an improved sliding mode observer for pmsm position servo system. IEEE Trans. Power Electron. **36**(3), 3211 (2020)

36. Paulo, S.D., et al.: Adaptive filtering: algorithms and practical implementation. Int. Ser. Eng. Computer Sci. **87**, 23–50 (2008)

37. Gorbet, R., Wang, D.W., Morris, K.A.: in *Proceedings. 1998 IEEE International Conference on Robotics and Automation (Cat. No. 98CH36146)*, vol. 3 (IEEE, 1998), vol. 3, pp. 2161–2167